



**HAL**  
open science

## Flame-vortex interaction: Effect of residence time and formulation of a new efficiency function

F. Thiesset, G. Maurice, F. Halter, Nicolas Mazellier, C. Chauveau, I. Gökalp

### ► To cite this version:

F. Thiesset, G. Maurice, F. Halter, Nicolas Mazellier, C. Chauveau, et al.. Flame-vortex interaction: Effect of residence time and formulation of a new efficiency function. Proceedings of the Combustion Institute, 2017, 36 (2), pp.1843 - 1851. 10.1016/j.proci.2016.06.172 . hal-01660275

**HAL Id: hal-01660275**

**<https://hal.science/hal-01660275v1>**

Submitted on 28 Mar 2019

**HAL** is a multi-disciplinary open access archive for the deposit and dissemination of scientific research documents, whether they are published or not. The documents may come from teaching and research institutions in France or abroad, or from public or private research centers.

L'archive ouverte pluridisciplinaire **HAL**, est destinée au dépôt et à la diffusion de documents scientifiques de niveau recherche, publiés ou non, émanant des établissements d'enseignement et de recherche français ou étrangers, des laboratoires publics ou privés.

# Flame-vortex interaction : effect of residence time and formulation of a new efficiency function

F. Thiesset<sup>a</sup>, G. Maurice<sup>a,b</sup>, F. Halter<sup>\*a</sup>, N. Mazellier<sup>b</sup>, C. Chauveau<sup>a</sup>, I. Gökalp<sup>a</sup>

<sup>a</sup>CNRS ICARE, Avenue de la Recherche Scientifique, 45072 Orléans Cedex 2 France

<sup>b</sup>University of Orléans, INSA de Bourges, PRISME, EA 4229, 45072 Orléans, France

---

## Abstract

In this study, a combined experimental and numerical investigation of a toroidal vortex interacting with a stagnation premixed flame is carried out with the aim of quantifying the ability of such a vortex to stretch the flame. By scrutinizing the literature, it was found that, although inferred from exactly similar numerical simulations, existing parametric expressions for the efficiency function (the ratio of the flame stretch to vortex strain) do not agree in the way the latter should behave when the ratio of the vortex rotational velocity  $U_\theta$  to the laminar flame speed  $S_L$  is increased. These expressions also appear to be unequally accurate when compared to experimental data and do not feature the non monotonic evolution of the efficiency function with  $U_\theta/S_L$  which is observed in both experimental data and numerical simulations of a 'isothermal' propagating interface. In addition, whilst previous studies have focused only on the impact of  $U_\theta/S_L$  and  $R_v/\delta_L$  ( $R_v$  being the vortex typical size and  $\delta_L$  the laminar flame thickness) our study reveals the importance of other parameters, the most important of which being the residence time of the vortex associated with its convection velocity. These results yield a new formulation for the efficiency function which compares favourably well with experimental data.

**Keywords:** Flame vortex interactions, Flame stretch, Vortex strain, residence time

---

---

\*Corresponding author at: CNRS ICARE, Avenue de la Recherche Scientifique, 45072 Orléans Cedex 2 France  
Email: fabien.halter@cnrs-orleans.fr (F. Halter)

\*\*Colloquium : TURBULENT FLAMES  
Total length = 6126 words (Method 2)  
Main text = 4231 words  
Nomenclature = 0 word  
References = 253 words  
Figure 1 to 10 = 198, 207, 132, 161, 136, 147, 191, 125, 191, 154 words  
Tables = 0 word  
No color reproduction

## 1. Introduction

Understanding and predicting the different mechanisms at play in turbulent premixed flames is a tremendously difficult challenge. The main reason is that there is still a lack of knowledge of the turbulent flow structure which features a large variety of turbulent scales. A given eddy thus experiences many different processes induced by turbulent scales of different sizes, such as vortex stretching and sweeping, diffusion by viscosity, these effects being particularly arduous to model. In addition, when reacting flows are concerned, the flame does not act as a passive scalar because of its propagative character and the inherent heat release that locally modifies the fluid physical properties. The high local flame curvature and strain, also impact its local consumption or displacement speed in a way which remains poorly understood.

There is thus a need for fundamental investigations of the interactions between the fluid motion and a flame in simplified and well controlled situations. One of these is the case of a flame interacting with a single vortex dipole (see the review by Renard et al. [1]). Pioneer studies of Flame-Vortex Interactions (hereafter abbreviated by FVI) emerged in the 90's with notably Poinot et al. [2], Roberts and Driscoll [3], Wu and Driscoll [4], Roberts et al. [5], Lee and Santavicca [6] and more recently with Renard et al. [1], Colin et al. [7], Charlette et al. [8], Bougrine et al. [9].

Although some effects such as vortex stretching, sweeping, tilting are not present, FVI are expected to mimic, at least partly, the processes at play in real turbulent flames. The aforementioned investigations on FVI have led notably to the construction of the so-called spectral diagrams which allows to identify the conditions needed for a vortex to stretch the flame, to create pockets of fresh gas or to locally quench the flame. In addition, these results yielded expression of efficiency functions, i.e. the transfer function between vortex strain and flame stretch. In this prospect, Colin et al. [7], Charlette et al. [8] have focused on the effect of vortex size  $R_v$  relative to the flame thickness  $\delta_L$  and vortex rotational velocity  $U_\theta$  relative to the flame speed  $S_L$ . More recently, the effect of Lewis number has been incorporated by Bougrine et al. [9]. These efficiency functions are extremely valuable as they are widely used in LES of turbulent premixed combustion in order to model the sub-grid scale wrinkling factor [7–9].

The aim of the present study is to explore one particular aspect of the interaction between the flow motion and a flame, which we referred to as the *strain-sweeping competition* (see for instance the review by Driscoll [10]). This competition can be conceptually described in terms of time-scales. Based on phenomenological arguments [11], the strain-based time scale  $\tau_s$  of a scale  $r$  with characteristic velocity  $u_r$  is  $\tau_s \propto r/u_r \propto r^{2/3}$ . This time-scale is generally referred to as the eddy turn-over time. Previous studies devoted to FVI investigations [2–9] indicate that the

smaller this time scale, the larger is the flame stretch. On the other hand, Tennekes [12] suggested that another relevant time scale in a turbulent flow relates to the sweeping effect by energy-containing eddies. He pointed out that a given scale of size  $r$  is convected by the large scales, i.e. with characteristic velocity of the order of  $u'$ , the root-mean-square of the velocity fluctuations. The sweeping time scale as called by Tennekes [12] thus writes  $\tau_c \propto r/u'$ . This has been verified experimentally by e.g. Poulain et al. [13]. It is worth stressing that these two phenomenology both lead to the same prediction for the scaling exponent of the energy spectra and are therefore undistinguishable in spectral space. In the field of combustion the sweeping time scale is somehow related to the residence time [10] and basically describes the duration of the interaction of a vortex located in the vicinity of the flame. As far as the sweeping (or residence) time scale is concerned, FVI [3, 4] corroborates the intuitive statement that the smaller this time scale, the smaller the flame stretch since the vortex spends less time in the vicinity of the flame for rolling it up. In turbulent flames, there is thus a competition between turbulent strain and turbulent convection, the latter phenomenon acts in decreasing the flame stretch whereas the former has the opposite effect. It is thus worth investigating these effects independently in order to give further insight into their respective influence on the flame. Further, a more complete expression for the efficiency function which accounts for both strain and residence time effects could be derived and used in LES.

In the present study, a new experimental set-up was designed in the goal of quantifying the degree of the interactions between a vortex dipole and a stagnation premixed flame. Some simple numerical simulations based on the 'isothermal' G-equation, have been further carried out and validated against experimental data. Such simulations allow to assess the effect of the convection velocity and rotational velocity independently. Finally, the respective effect of these two phenomena on flame stretch are separately quantified, incorporated into a new formulation for the efficiency function, and compared to experimental data.

## 2. Experimental apparatus

Investigations are carried out in a single jet stagnation flame configuration which is a modified version of that used by Bouvet et al. [14]. A schematic of the burner is provided in Fig. 1. A laminar strained flame is stabilized against a 4-mm-thick stainless steel plate. The stagnation plate is attached to an alumina foam plug selected for its insulating properties. The fuel and oxidizer are introduced through the side of the burner. A so-called 'particle diffuser cone' filled with 6 mm glass beads is used to ensure a homogeneous mixture in the nozzle plenum. The reactive mixture then flows into the burner plenum through a 5 mm thick aluminium grid. It is finally accelerated in the

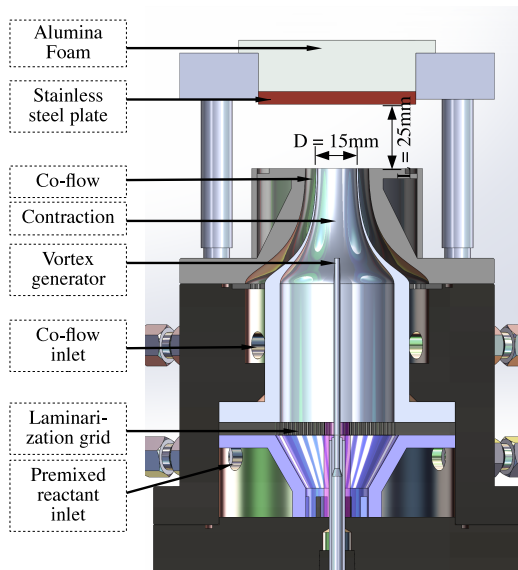


Figure 1: Schematic of the experimental setup

119 converging section with a  $D = 15\text{mm}$  outflow diame-  
 120 ter, creating an upward-oriented jet with a nearly top  
 121 hat velocity profile at the burner exit. The burner-to-  
 122 stagnation plate distance  $L$  was fixed to  $25\text{mm}$ , given a  
 123  $L/D$  ratio greater than unity as usually recommended.  
 124 Moreover, it allows to stabilize flames sufficiently far  
 125 from the plate to track the flame/vortex interaction  
 126 without being affected by the plate. To avoid external  
 127 perturbations and improve flame stability, a laminar  
 128 coaxial shroud of nitrogen is used. The nitrogen flow  
 129 rate was set so that the coflow exit velocity closely  
 130 matches that of the main flow. In the present study,  
 131 the wall stagnation configuration is preferred over the  
 132 classical opposed jet configuration for the following  
 133 reasons: (i) the experimental apparatus can be im-  
 134 plemented and controlled easily (no need for upper  
 135 burner) and (ii) wall-stabilized flames are generally  
 136 found to be more stable than counterflow ones.

137 The toroidal vortex is generated by applying a sud-  
 138 den pressure discharge of reactive mixture of same  
 139 equivalence ratio than the main flow in a tube of  $2\text{mm}$   
 140 in diameter located on the centerline of the flow and  
 141  $35\text{mm}$  upstream the burner outlet (Fig. 1). The in-  
 142 tensity of the vortex is controlled by varying the pres-  
 143 sure magnitude within a pressurized tank located up-  
 144 stream. To control the duration of the pressure dis-  
 145 charge, it was necessary to use two electro-valves  
 146 placed one after another because the time needed for  
 147 a single electro-valve to open and close was too large.  
 148 First, the upstream electro-valve is kept closed while  
 149 the second placed downstream is opened. Then, for  
 150 generating the vortex, the first valve is opened while  
 151 the second one is closed with a small time delay, so  
 152 that the pressure discharge duration was about  $5\text{ms}$ .

153 Three equivalence ratios for the reactive methane-  
 154 air mixture  $\phi = 1, 0.9, 0.8$  have been considered. The

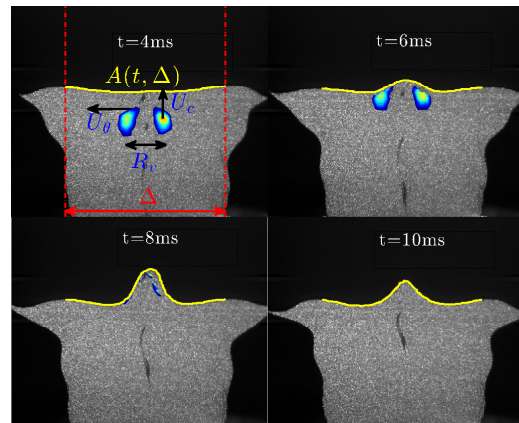


Figure 2: Time sequence of Mie scattering images of a typical FVI ( $U_\theta/S_L = 1.43$ ). The flame contours and vorticity field are superimposed. The top of each image has been cropped to show only the first  $20\text{mm}$ . The line corresponds to the flame contours with area  $A(t, \Delta)$  estimated over a domain of width  $\Delta$ .  $U_\theta$ ,  $U_c$  are the vortex rotational and convection respectively, whilst  $R_v$  is the vortex core-to-core distance.

155 laminar flame speed and thickness have been evalu-  
 156 ated using the GRI-mech 3.0 mechanism together with  
 157 the stagnation flame module of the CHEMKIN  
 158 Pro software. The temperature of the wall, measured  
 159 by Bouvet et al. [14], was set to  $800\text{K}$ . It was found  
 160 that  $S_L = 40.3, 36.5, 30.6\text{cm}\cdot\text{s}^{-1}$  and  $\delta_L = 433, 463,$   
 161  $525\mu\text{m}$  respectively for  $\phi = 1, 0.9$  and  $0.8$ . The strain  
 162 rate was respectively  $90, 86$  and  $77\text{s}^{-1}$  for  $\phi = 1, 0.9$   
 163 and  $0.8$ .

164 The flame front is tracked by means of Mie scatter-  
 165 ing laser tomography. Seeding of the flow is made  
 166 by silicon oil droplets supplied by an atomizer. Typ-  
 167 ical size of droplets is about  $1\mu\text{m}$ . It was checked  
 168 that the flame location was the same when the seeding  
 169 was turned off suggesting that the laminar flame speed  
 170 was not altered by the addition of silicon droplets in  
 171 the flow. Then, use is made of a continuous Coherent  
 172 Verdi G20 Laser which delivers up to  $20\text{W}$  at  $532\text{nm}$ .  
 173 The light scattered by the droplets is then captured by  
 174 a Phantom V1210 camera, equipped with a  $105\text{mm}$   
 175  $\text{F}2.8$  lens, working at an acquisition rate of  $23005\text{Hz}$   
 176 with a field of view of  $704 \times 640$  pixels<sup>2</sup> and the resolu-  
 177 tion was  $38\mu\text{m}/\text{px}$ .

178 The flame contour is then extracted as follows.  
 179 Firstly, a contrast-limited adaptive histogram equal-  
 180 ization (CLAHE) is applied to the original images in  
 181 order to optimize the contrast in the images. Then, to  
 182 limit the pixelization associated with the CLAHE, im-  
 183 ages are filtered using a Gaussian filter of size equal  
 184 to 4 times the spatial resolution. For the binarizing  
 185 procedure, we use a standard threshold-based tech-  
 186 nique. More precisely, the histogram of the gray scale  
 187 is calculated. The latter reveals two distinct peaks  
 188 corresponding to the fresh and burned gas respectively.  
 189 The threshold value for discriminating the flame con-

190 tour is set as the average value between the gray scale  
 191 of these two peaks. This yields estimations for the  
 192 progress variable, noted  $c$ , which is by definition 0 and  
 193 1 in the unburned and burned gas respectively. The ve-  
 194 locity field within the unburned mixture is estimated  
 195 by classical 2D-2C Particle Image Velocimetry (PIV).  
 196 For this purpose, the Matlab subroutines of Thielicke  
 197 and Stamhuis [15] were used. A time sequence of Mie  
 198 scattering images at four distinct instants is shown in  
 199 Fig. 2. The vorticity field and flame contours are su-  
 200 perimposed. The time  $t_0 = 0$  was set arbitrarily as the  
 201 time  $t$  where the vortex center was 2.5mm downstream  
 202 the burner outlet. One observes that at a time  $t=4$ ms,  
 203 the flame is rather flat suggesting that the vortex gen-  
 204 erator is sufficiently far from the burner outlet for not  
 205 creating a wake. As the vortex is convected ( $t=6$ ms  
 206 and 8ms), the flame is increasingly stretched. Its area  
 207 then reaches a maximum before decreasing ( $t=10$ ms)  
 208 while the flame goes back to its original position.

209 The vortex parameters, i.e. the circumferential ve-  
 210 locity  $U_\theta$ , the convection velocity  $U_c$  and the core-  
 211 to-core distance  $R_v$ , have been inferred from PIV by  
 212 fitting the velocity field calculated with an Oseen vor-  
 213 tex. Our experimental set-up allows to cover the  
 214 range  $0.5 \lesssim U_\theta/S_L \lesssim 2.5$  whereas  $R_v/\delta_L$  slightly  
 215 varies around 6.5. Our database thus lies between  
 216 the no-effect limit and the quenching limit assessed  
 217 by Roberts et al. [5].

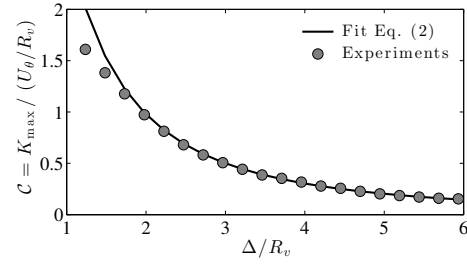
### 218 3. Experimental results

#### 219 3.1. Domain size effects

220 The focus of this paper is on the flame stretch as-  
 221 sociated with the interaction with a vortex. Given the  
 222 vortex rotational velocity  $U_\theta$  and the distance between  
 223 vortex cores  $R_v$  (see Fig. 2), the vortex strain is gener-  
 224 ally estimated as  $U_\theta/R_v$  [7–9]. On the other hand, the  
 225 flame stretch is evaluated as

$$226 K(t, \Delta) = \frac{1}{A(t, \Delta)} \frac{\partial A(t, \Delta)}{\partial t} \quad (1)$$

227 where, thanks to axisymmetry,  $A(t, \Delta) =$   
 228  $\int y(s) \sqrt{x'^2 + y'^2} ds$  is the flame area at a time  $t$   
 229 evaluated over a domain of width  $\Delta$  (see Fig. 2).  
 230  $s$  is the curvilinear parameter,  $y$  and  $x$  are the  
 231 flame contour spatial coordinates and the prime  
 232 denotes derivatives with respect to  $s$ . Then the  
 233 efficiency function is defined as in [7–9], viz.  
 234  $C(\Delta) = K_{\max}(\Delta)/(U_\theta/R_v)$ , where  $K_{\max}(\Delta)$  is the  
 235 maximum value of  $K(t, \Delta)$ . The appearance of  
 236  $\Delta$  in the efficiency function is new. In previous  
 237 numerical studies [7–9] a given value for  $\Delta \approx 6R_v$   
 238 corresponding to the size of the simulation domain  
 239 was chosen. However, it appears straightforward  
 240 that  $K_{\max}$  depends on  $\Delta$ . Indeed, because the portion  
 241 of flame interacting with the vortex is constant (i.e.  
 242 there exists a  $\Delta$  above which  $\partial A/\partial t$  is independent of  
 243  $\Delta$ ), we expect  $K_{\max}$  to decrease with  $\Delta^2$  since  $A(t, \Delta)$   
 244 monotonically increases with  $\Delta^2$ . Figure 3 presents



244 Figure 3: Evolution of  $K_{\max}$  with  $\Delta$  for  $U_\theta/S_L = 1.43$ . Sym-  
 245 bols represent experimental data whilst the line corresponds  
 246 to the fit using Eq. (2).  
 247

244 the evolution of  $K_{\max}$  with respect to  $\Delta$ . It clearly  
 245 appears that  $K_{\max}$  rapidly decreases with respect to  
 246  $\Delta$  and for  $\Delta$  sufficiently large (i.e. for  $\Delta$  larger to a  
 247 certain  $\Delta_i$ ), it is found that  $K_{\max}$  follows the relation

$$248 K_{\max} = K_{\max}^0 \left[ \frac{\Delta_i - \Delta_0}{\Delta - \Delta_0} \right]^2. \quad (2)$$

249 In Eq. (2),  $\Delta_i$  represents the domain width above  
 250 which  $\partial A/\partial t$  is constant and  $\Delta_0$  is interpreted as a vir-  
 251 tual origin, i.e.  $K_{\max}^{-1} \rightarrow 0$  when  $\Delta \rightarrow \Delta_0$ . From our  
 252 experimental database, it was found that  $\Delta_i/R_v$  and  
 253  $\Delta_0/R_v$  were constant and are equal to  $2.5 \pm 0.05$  and  
 254  $-0.5 \pm 0.1$  respectively.

255 Figure 3 emphasizes that the values for the effi-  
 256 ciency function that were previously provided notably  
 257 by Colin et al. [7], Charlette et al. [8], Bougrine et al.  
 258 [9], were inferred for a given value of  $\Delta/R_v$  whereas  
 259 they should depend on  $\Delta$ . In other words, if they had  
 260 chosen a different value for the simulation domain,  
 261 they would have obtained different values. Moreover,  
 262 the no-effect limit assessed by Poinso et al. [2] which  
 263 "corresponds to vortices which induce a maximum  
 264 modification of the total reaction rate of about 5 per-  
 265 cent", should also depend on  $\Delta$ .

#### 266 3.2. Impact of vortex intensity

267 We now turn our attention to the effect of the vor-  
 268 tex strength on the flame stretch. Figure 4 depicts the  
 269 evolution of  $C^0 = K_{\max}^0/(U_\theta/R_v)$  as a function  $U_\theta/S_L$   
 270 (hereafter the superscript  $0$  on  $C$  will be removed for  
 271 the sake of simplicity). Experimental results are also  
 272 compared to the predictions provided by Colin et al.  
 273 [7], Charlette et al. [8], Bougrine et al. [9] which are  
 274 respectively noted  $C_{co}$ ,  $C_{ch}$  and  $C_b$ . Their respective  
 275 analytical expressions are not recalled here but the  
 276 reader can refer to [7–9] for more details.

277 Experimental uncertainties have been estimated as  
 278 follows. The precision of the subpixel interpolation of  
 279 the PIV algorithm is generally about 0.05 pixel. The  
 280 uncertainty on the velocity field is therefore constant  
 281 and equals to about  $0.04 \text{ m.s}^{-1}$  provided the resolution  
 282 and sampling frequency of our images. The error on  
 283 the estimation of  $R_v$  provided by fitting experimental

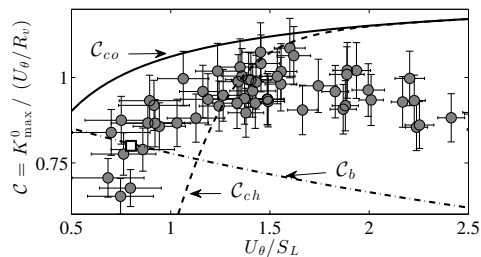


Figure 4: Efficiency function  $C = K_{\max}^0 / (U_\theta / R_v)$  as a function of  $U_\theta / S_L$ . The lines labeled  $C_{co}$ ,  $C_{ch}$ ,  $C_b$  correspond respectively to the parametric expressions provided by Colin et al. [7], Charlette et al. [8], Bougrine et al. [9], corrected using Eq. (2) to obtain  $K_{\max}^0$ . The circle symbols correspond to the present measurements whilst the square symbol is taken from Bougrine et al. [9]

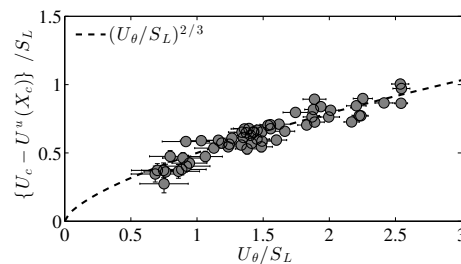


Figure 5: Convection velocity  $U_c - U^u(X_c)$ , where  $U^u(X_c)$  is the streamwise velocity of the unperturbed flow at the vortex center location  $X_c$ , as a function of  $U_\theta$ . The dotted line is given by  $0.5(U_\theta / S_L)^{2/3}$ .

283 data with an Oseen vortex was generally of about 4%.  
 284 The uncertainty in the determination of  $K_{\max}$  was supposed to be negligible by comparison with the errors  
 285 on both  $U_\theta$  and  $R_v$  since  $A$  is readily measurable.

286  
 287 A careful analysis of Fig. 4 first reveals that, although rather limited, some departures between exper-  
 288 imental data and the predictions of either [7–9] can be observed. By comparison with experiments,  
 289 the efficiency function of Colin et al. [7] appears to be the more appropriate. These differences might be  
 290 explained by several parameters. First, it is worth recalling that our configuration is axisymmetric whilst  
 291 DNS of [7–9] are 2D (planar). Secondly, in [7–9], the flame stretch is estimated from the heat release  
 292  $Q$ , i.e.  $K = Q^{-1} dQ/dt$  which implicitly suggests that Refs. [7–9] considered that the flame consumption  
 293 speed was unaltered by the flame stretch. Such an hypothesis is consistent with LES models based  
 294 on the flame density concept for which the heat release or fuel consumption is calculated through the  
 295 laminar flame speed multiplied by the flame surface density. This assumption is however not consistent  
 296 with LES that employs skeletal or analytical chemistry which explicitly accounts for the effect of stretch  
 297 on the flame consumption speed.

298  
 299 Fig. 4 also suggests that though based on exactly similar simulations, existing parametric expressions  
 300 do not agree in the way  $C$  should behave with respect to  $U_\theta / S_L$ . Indeed, Colin et al. [7], Charlette  
 301 et al. [8] both predict an increasing tendency of  $C$  with respect to  $U_\theta / S_L$  whereas  $C_b$  leads to the oppo-  
 302 site trend. Although slightly scattered, our experimental data further suggest that the evolution of  $C$  is  
 303 non monotonic, i.e.  $C$  first increases before decreasing slightly for  $U_\theta / S_L$  larger than about 1.5. The decreasing  
 304 tendency of  $C$  was also observed in the DNS of Bougrine et al. [9] when the vortex strength was en-  
 305 hanced from  $U_\theta / S_L = 0.8$  to 8 (note that there is a nice agreement between our experiments and the DNS data  
 306 of Bougrine et al. [9] for  $U_\theta / S_L = 0.8, R_v / \delta_L = 5$ ). This observation can be readily explained by recalling

324 that an intense vortex will create high local curvatures which act in decreasing the total stretch of the flame.  
 325 In other words, increasing the vortex strength can be less efficient since it leads to too high curvatures that  
 326 globally reduces the flame stretch.

327  
 328 Roberts and Driscoll [3] were first to realize that the flame stretch is also driven by the convection velocity  
 329  $U_c$  of the vortex dipole. More precisely, they suggested that for a given  $U_\theta$ , increasing  $U_c$  yields  
 330 a smaller flame stretch because the residence time of the vortex in the vicinity of the flame decreases. This  
 331 intuitive statement was further confirmed by Wu and Driscoll [4] on the basis of numerical simulations of  
 332 a propagating surface. There is thus a need for incorporating these two opposed effects (convection vs rota-  
 333 tional velocity) into a more complete expression of the efficiency functions. However, in our experiments,  
 334 it was observed that increasing  $U_\theta$  irremediably led to a higher convection velocity consistently with analyt-  
 335 ical studies (see [1] and references therein). It was found experimentally (Fig. 5) that the convection velocity  
 336  $U_c - U^u(X_c)$  ( $U^u$  the streamwise velocity experienced by the vortex located at  $X_c$ ) scales as  $U_\theta^{2/3}$ .  
 337 Therefore, it is not possible from experiments to assess independently the respective influence of  $U_\theta$  and  
 338  $U_c$ .

339  
 340 Consequently, following e.g. Wu and Driscoll [4] or Lee and Santavica [6], we decided to perform sim-  
 341 plified numerical simulations of the same burner in the goal of studying the effect of  $U_c$  and  $U_\theta$  indepen-  
 342 dently. These simulations have been widely used in the past mainly because they are extremely low-cost  
 343 in terms of computational resources. Indeed, they consider the flame as a ‘passive’ propagating (ther-  
 344 mally neutral) interface, which tremendously reduces the problem complexity. Such simulations neglect the  
 345 heat release and therefore many physical mechanisms are not taken into account. First, the higher viscosity  
 346 due to high temperature in the burnt gas, resulting in a larger dissipation rate is not accounted for. Baro-  
 347 clinic effects as evidenced by [5] are also neglected. However, with this limitations in mind, one aspect of  
 348 the present work is to investigate in detail how real-

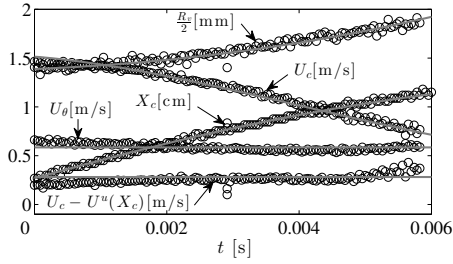


Figure 6: Time evolution of the vortex parameters for a given case in the database. The vortex core-to-core distance  $R_v$ , the convection velocity  $U_c$  and  $U_c - U^u(X_c)$ , the vortex center streamwise position  $X_c$ , and the rotational velocity (black) are represented as a function of time. Symbols are experimental data whilst lines stand for the simulation.

367 istic these (widely used) simulations could be when  
 368 compared to experiments. In other words, handling  
 369 such a comparison helps in giving further insights into  
 370 the importance of heat release and associated physical  
 371 mechanism during a FVI.

## 372 4. Simulations of a vortex interacting with a 373 propagating interface

### 374 4.1. Implementation and validation

375 Present numerical simulations consider the flame  
 376 as a two-dimensional (axisymmetric) propagating inter-  
 377 face convected by the fluid motion  $\mathbf{U}$  while advancing  
 378 at the laminar flame speed  $S_L$ . The kinematic relation-  
 379 ship between the flame and the flow field is then  
 380 given by the G-equation which writes [4, 6]

$$\frac{\partial G}{\partial t} + \mathbf{U} \cdot \nabla G = S_L |\nabla G|. \quad (3)$$

381 In the present case, the Navier-Stokes are not explicitly  
 382 resolved and the velocity field is set as follows. First,  
 383  $U^u$  and  $V^u$ , i.e. the velocity component  
 384 in the streamwise  $x$  and transverse  $y$  direction of un-  
 385 perturbed flow (before the generation of the vortex)  
 386 is given by  $U^u(x, y) = -2 \int a(x) dx$  and  $V^u(x, y) =$   
 387  $a(x) \times y$ , where  $U_0 = 1.23 \text{ m} \cdot \text{s}^{-1}$  is the inlet velocity  
 388 of the burner and  $a(x) = \partial V^u / \partial y (y = 0)$  is the trans-  
 389 verse strain of the unperturbed flow.  $a(x)$  was fitted  
 390 from experiments using a second order polynomial.  
 391 The coefficients of the polynomial were adjusted for  
 392 each equivalence ratio.

393 Secondly, the vortex velocity field was added to  $U^u$   
 394 and  $V^u$  and set using the Oseen expression. The input  
 395 parameters for the Oseen vortex are  $U_\theta$ ,  $X_c$  (the  
 396 streamwise location of the vortex center) and  $R_v$ , the  
 397 core-to-core distance. In the present case, by analyzing  
 398 experimental data (see Fig. 6), it was found that  
 399  $U_\theta$  does not vary with time and was therefore set to  
 400 a constant. The vortex center  $X_c$  was convected at a  
 401 velocity  $U_c$ , viz.  $\partial X_c / \partial t = U_c$ , where  $U_c - U^u(X_c)$

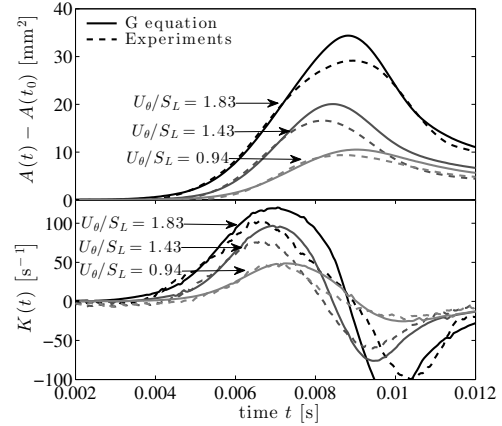


Figure 7: Time evolution of the flame area  $A(t, \Delta)$  (a) and stretch  $K(t, \Delta)$  (b) for  $\Delta = 10 \text{ mm}$ , for three different ratio of  $U_\theta/S_L = 0.94, 1.43, 1.83$ . Dashed and full lines correspond respectively to experimental and numerical data

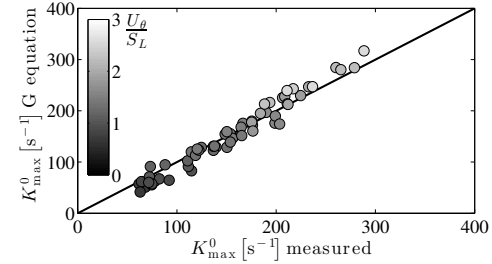


Figure 8: Maximum stretch  $K_{\max}^0$  assessed by experiments versus  $K_{\max}^0$  inferred from numerical simulations. Symbols are coloured by  $U_\theta/S_L$

402 was found to be constant (see Fig. 6). The time evolu-  
 403 tion of the vortex ring diameter  $R_v$  follows the relation  
 404 [16]  $R_v^{-1} \partial R_v / \partial t = a(X_c)$ . In Fig. 6, the time evolu-  
 405 tion of vortex parameters issued from the experiments  
 406 are compared to that prescribed in the numerical simu-  
 407 lations. All quantities compare extremely well and  
 408 thus validate the procedure for establishing the velocity  
 409 field.

410 The  $G$ -field was initialized as a signed distance  
 411 with the iso-value  $G = G_0 = 0$  located at the  
 412 streamwise location  $x$  at which  $U^u(x) = S_L$ . Equa-  
 413 tion (3) is resolved using a fifth-order WENO discreti-  
 414 zation scheme in space and 4th-order Runge-  
 415 Kutta scheme for time advancement. The usual reini-  
 416 tialization procedure is also applied at each time step  
 417 so that the  $G$ -field remains a signed distance. The  
 418 mesh size is  $500 \times 500$  corresponding to a domain  
 419 size of  $25 \times 25 \text{ mm}^2$ . It was checked that increasing  
 420 the mesh size up to  $1000 \times 1000$  points yielded only  
 421 marginal differences.

422 Numerical simulations have been validated against  
 423 experimental data. Results for three different values

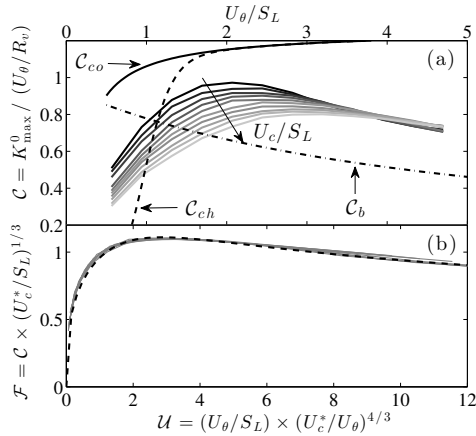


Figure 9: (a) Efficiency function as a function of  $U_\theta/S_L$  for different values of  $U_c/S_L$ . The arrow indicates increasing values of  $U_c/S_L$ . (b) Rescaled efficiency function as a function of a rescaled velocity ratio. The black dashed line represent the fit using Eq. (4)

of  $U_\theta/S_L = 0.94, 1.43, 1.83$  are presented in Fig. 7. The increase of  $A(t, \Delta)$  is very nicely reproduced by the simulation, whilst some slight departures are observed close to the maximum of  $A(t, \Delta)$ . This indicates that the early stage of the interaction (i.e. before the vortex reaches the burnt gas) relies mainly on a kinematic interaction and that the heat release does not play a significant role at this stage. The simulated flame stretch compares favourably well with experiments for the three cases represented in Fig. 7. A scatter plot between the measured and simulated  $K_{\max}^0$  for the entire database is further given in Fig. 8. Here again, a nice agreement is observed. Departures between numerical and experimental data for  $K_{\max}^0$  lies within 20% on average.

#### 4.2. Formulation of a new efficiency function

By use of such numerical simulations, the effect of  $U_c$  and  $U_\theta$  on  $K_{\max}^0$  can thus be studied independently with the aim of incorporating these parameters in a more complete expression for the efficiency function.

In Fig. 9(a), are provided the numerical results for the efficiency function as a function of  $U_\theta/S_L$  for  $0.6S_L \leq U_c - U^u(X_c) \leq 4.7S_L$ . Noticeable is the non monotonic evolution of  $C$  with respect to  $U_\theta/S_L$  that was previously observed in the experiments (see Fig. 4). Furthermore, one clearly sees a dependence of  $C$  on  $U_c$ . Note that for  $U_\theta/S_L > 3.5$  the effect of  $U_c$  is almost negligible. In Fig. 9(b), it is shown that the evolution of  $C$  with respect to  $U_c$  and  $U_\theta$  can collapse on a single curve, when the rescaled efficiency function  $\mathcal{F} = C \times (U_c^*/S_L)^{1/3}$  is plotted as a function of a rescaled velocity ratio  $\mathcal{U} = (U_\theta/S_L) \times (U_c^*/U_\theta)^{1/3}$ , where  $U_c^* = U_c - U^u(X_c) + S_L$  is the relative velocity between the flame and the vortex centers [4]. This curve highlights a first zone for  $\mathcal{U} < 2.5$  where

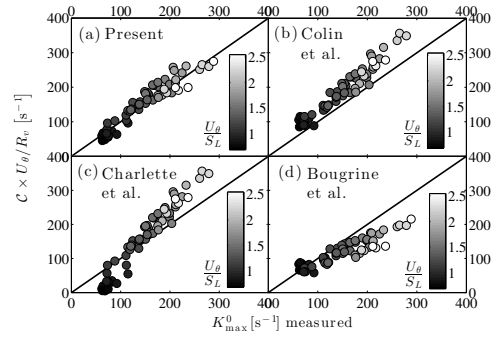


Figure 10: Scatter plot of the experimental vs modelled flame stretch using the present efficiency function (a), that of Colin et al. [7] (b), Charlette et al. [8] (c) and Bougrine et al. [9] (d). Symbols are coloured by  $U_\theta/S_L$

$\mathcal{F}$  scales as  $\mathcal{U}^{1/3}$ , and a second zone at larger  $\mathcal{U}$  for which  $\mathcal{F}$  decreases as  $\mathcal{U}^{-1/4}$ . This trend can be well fitted by the following parametric expression (the black dashed line in Fig. 9(b))

$$\mathcal{F} = \mathcal{U}^{1/3} \left[ 1 + \left( \frac{\mathcal{U}}{\mathcal{U}_{\max}} \right)^2 \right]^{-\frac{7}{24}}, \quad (4)$$

from which  $C = \mathcal{F} \times (U_c^*/S_L)^{-1/3}$  can be recovered.  $\mathcal{U}_{\max}$  is the rescaled velocity ratio for which the bending of  $\mathcal{F}$  is observed and was found to be equal to 2.5. The ability of this expression for modelling the flame stretch from the vortex strain is emphasized in Fig. 10. Departures between modelled and measured  $K_{\max}^0$  are similar to Fig. 8, i.e. within 20%. The present formulation for  $C$  further appears to be more adequate than either that of Colin et al. [7], Charlette et al. [8] or Bougrine et al. [9].

## 5. Conclusion

The present study is devoted to the exploration of the flame stretch induced by a vortex dipole with special emphasis on the *strain-sweeping competition*. Both experiments and numerical simulations of a stagnation flame have been carried out, with the aim of assessing the ability of available parametric expression for describing the efficiency function. The outcomes of the present study can be summarized as follows:

- It was first shown that, though based on the same numerical data,  $C$  provided by both Colin et al. [7], Charlette et al. [8] predict an increase of  $C$  with respect to  $U_\theta/S_L$  whereas that of Bougrine et al. [9] emphasizes the opposite trend. In addition, all these expressions fail in describing the non-monotonic evolution of  $C$  with respect to  $U_\theta/S_L$  which is observed in both experimental and numerical data.



491 • Secondly, by comparing experiments to simplified numerical simulations based on the 'isothermal' G-equation, it was shown that the early stage of interaction is driven by a kinematic interaction between the vortex and the flame. The maximum flame stretch issued from such numerical simulations is in agreement with experiments.

499 • Finally, these simulations allow the effect of the residence time of the vortex in the vicinity of the flame to be investigated. A new parametric expression for the efficiency function is proposed and compares favourably well with experimental data.

505 As mentioned in the introduction, strain and sweeping effects are respectively representative of rather small ( $u_r$ ) and large scales ( $u'$ ) phenomena. This indicates *a priori* that in a LES,  $C$  can be evaluated, using the sub-grid scale velocity for  $U_\theta$  and the total (resolved + sub-grid scale) velocity for  $U_c$ . The residence time also requires the knowledge of the vortex sweeping direction compared to the flame normal direction, for which a sub-model has yet been developed. Another important point concerns the fact that in LES, the efficiency functions have to be integrated over all the sub-grid scales. In previous studies, e.g. [8], the integration was done in spectral space. It is worth stressing that the integration over available turbulent scales might not be necessary by keeping the description in physical space (that of the structure or correlation functions), in which the notion of cumulative over turbulent scales is implicit (see e.g. [17]). Indeed, in Ref. [17], use was made of an expression for the turbulent strain (Eq. (1) in [17]) which represents the strain due to the combined effect of all smaller scales (as the structure function does, see e.g. [18] p.11, or [19] p 366). This expression is thus equivalent to the subgrid scale strain. Consequently, the multiplication of the efficiency function by the latter expression for the strain directly represents the flame stretch of all smaller scales than the scale considered. i.e. the subgrid flame stretch and there is no need for spectral integration.

534 Further work will be devoted to exploring the impact of the ratio  $R/\delta_L$  on  $C$  by changing the diameter of the vortex generator. We also plan to study in detail the effect of fuel composition and especially the Lewis number effects.

## 539 Acknowledgements

540 The financial support from the Agence National de la Recherche under the project IDYLLE is gratefully acknowledged. In this respect, we would like to thank especially S. Richard, L. Selle and T. Poinso for fruitful discussions. We are also thankful to the CNRS, the University of Orléans, and the French Government Program "Investissements d'avenir" through the LABEX CAPRYSES. FT acknowledges EADS for

its financial support. We also benefited from the computing resources provided by CaSciModOT. We thank Laurent Catherine for his technical assistance. We are grateful to Seong Young Lee for providing us the CHEMKIN PRO results.

## References

- [1] P.-H. Renard, D. Thevenin, J.-C. Rolon, S. Candel, *Prog. Energ. Combust.* 26 (2000) 225–282.
- [2] T. Poinso, D. Veynante, S. Candel, *J. Fluid Mech.* 228 (1991) 561–606.
- [3] W. L. Roberts, J. F. Driscoll, *Combust. Flame* 87 (1991) 245–256.
- [4] M.-S. Wu, J. F. Driscoll, *Combust. Flame* 91 (1992) 310–322.
- [5] W. L. Roberts, J. F. Driscoll, M. C. Drake, L. P. Goss, *Combust. Flame* 94 (1993) 58–69.
- [6] T.-W. Lee, D. Santavicca, *Combust. Sci. Technol.* 90 (1993) 211–229.
- [7] O. Colin, F. Ducros, D. Veynante, T. Poinso, *Phys. Fluids* 12 (2000) 1843–1863.
- [8] F. Charlette, C. Meneveau, D. Veynante, *Combust. Flame* 131 (2002) 159–180.
- [9] S. Bougrine, S. Richard, O. Colin, D. Veynante, *Flow, turbul. combust.* 93 (2014) 259–281.
- [10] J. F. Driscoll, *Prog. Energ. Combust.* 34 (2008) 91–134.
- [11] A. Kolmogorov, *Proc. USSR Ac. of Sci.* 30 (1941) 299–303.
- [12] H. Tennekes, *J. Fluid Mech.* 67 (1975) 561–567.
- [13] C. Poulain, N. Mazellier, L. Chevillard, Y. Gagne, C. Baudet, *Eur. Phys. J. B* 53 (2006) 219–224.
- [14] N. Bouvet, D. Davidenko, C. Chauveau, L. Pillier, Y. Yoon, *Combust. Flame* 161 (2014) 438–452.
- [15] W. Thielicke, E. J. Stamhuis, *Journal of Open Research Software* 2 (2014) 30.
- [16] R. Trieling, J. Van Wesenbeeck, G. Van Heijst, *Phys. Fluids* 10 (1998) 144–159.
- [17] F. Thiesset, G. Maurice, F. Halter, N. Mazellier, C. Chauveau, I. Gökalp, *Combustion Theory and Modelling* 20 (2016) 1–17.
- [18] A. A. R. Townsend, *The structure of turbulent shear flow*, Cambridge Univ Press, 1976.
- [19] P. A. Davidson, *Turbulence: an introduction for scientists and engineers*, Oxford University Press, 2015.